(c)2000 American Institute of Aeronautics & Astronautics or Published with Permission of Author(s) and/or Author(s)' Sponsoring Organization.

36th AIAA/ASME/SAE/ASEE Joint
Propulsion Conference & Exhibit
16-19 July 2000 Huntsville, AL

A00-36711

AIAA-2000-3521

Spacecraft Interaction Test Results of the High Performance Hall System SPT-140

J. M. Fife and W. A. Hargus, Jr.
U. S. Air Force Research Laboratory
Edwards AFB, CA

D. A. Jaworske, C. Sarmiento, L. Mason, and R. Jankovsky
NASA Glenn Research Center
Cleveland, OH

J. S. Snyder and S. Malone
Space Systems/Loral
Palo Alto, CA

J. Haas and A. Gallimore
University of Michigan
Ann Arbor, MI

Ground tests were performed to help characterize modes of interaction between the SPT-140 Hall thruster and spacecraft components. The experiments were performed at NASA Glenn Research Center and at the University of Michigan. Measurements were made of thruster plume current density, electromagnetic interference (EMI), and surface sputtering and contamination. Diagnostics included Faraday probes, collimated sputter/deposition targets, and radio-frequency detectors. Ion current density measurements showed exponential decay with off-axis angle up to approximately 30 degrees. At off-axis angles greater than 30 degrees, results varied with chamber background pressure, presumably due to ambient charge exchange plasma. Sputter rates of solar cell coverglass, Kapton, and RTV were accurately measured 1 m from the thruster exit for off-axis angles less than 60 degrees. At off-axis angles greater than 60 degrees, the sputter rate was on the order of the measurement uncertainty. EMI tests found very little emission in the traditional RF communication bands. At the lowest frequencies, one band of E-field emission (10 kHz to 20 MHz) was detected which exceeded the MIL-STD-461C specification by up to 53 dB.

Introduction

Owing to their high efficiency, optimal specific impulse, and relative simplicity, Hall thrusters have been used extensively on Russian spacecraft. As electric propulsion is becoming a more acceptable option on U.S. spacecraft, Hall thrusters are being considered for orbit topping, stationkeeping, and repositioning missions.

Most existing flight unit Hall thrusters operate at powers between 500 and 1600 Watts. Hall thrusters with higher powers, on the other hand, can be used more effectively for the dual mission of orbit topping and stationkeeping of geosynchronous spacecraft. For constant orbit-topping trip time, higher power Hall thrusters can yield significant gains in payload fraction to geosynchronous orbit.[1]

The High Performance Hall System (HPHS) is a complete 4.5-kW Hall-effect spacecraft propulsion system being developed under a cost-shared agreement between the U.S. Air Force and Atlantic Research Corporation. The goal of the HPHS program is to develop and demonstrate a Hall propulsion system capable of meeting the Integrated High Payoff Rocket Propulsion Technology (IHPRPT) Phase I Goals. The target performance of the system is:

Thruster Specific Impulse	1800 seconds
Overall System Efficiency	51%
Specific Mass (Thruster, PPU)	6.0 kg/kW
Life	7200 hours

A key element of HPHS is the SPT-140 Hall thruster, which is being developed by Engineering Design Bureau (EDB) Fakel in Kaliningrad, Russia. Under the HPHS program, a series of risk reduction tests was conducted in the U.S. using the SPT-140 Demonstration Model 3 (DM3). The DM3 had accumulated 8 hours during acceptance testing in Russia. It was then shipped to the U.S. where it underwent the testing reported in this paper, which involved 155 hours of additional firing.

Three categories of testing were performed to help quantify the integration effects of an SPT-140 Hall thruster with spacecraft. The first test series, performed at NASA Glenn Research Center (GRC)

This paper is declared a work of the U.S. Government and is not subject to copyright protection in the United States.

(c)2000 American Institute of Aeronautics & Astronautics or Published with Permission of Author(s) and/or Author(s)' Sponsoring Organization.

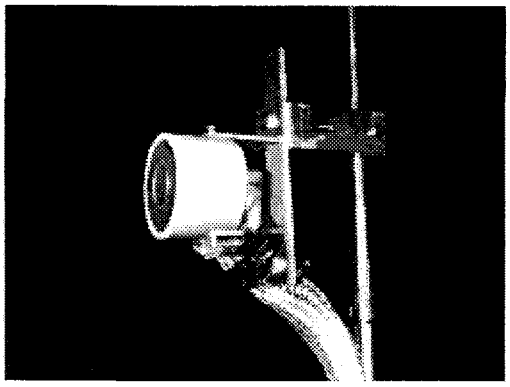

Fig. 1. Photograph of AFRL Faraday probe.

from 8/6/99 to 9/7/99, included performance, sputtering and contamination, and electromagnetic interference (EMI) tests. The second test series, performed at the University of Michigan Plasmadynamics and Electric Propulsion Laboratory (PEPL) from 9/20/99 to 9/28/99, included plume characterization tests. Condensed results from the plume characterization, sputtering and contamination, and EMI tests are presented in this paper. The results of the performance tests will be presented in a separate paper.[2]

Facility Descriptions

Tests at NASA GRC were performed in Vacuum Facility #6 (VF-6). VF-6 is a 21-m long by 8-m diameter, horizontal vacuum chamber located in the Electric Propulsion Laboratory at GRC. The chamber is cryogenically pumped at a speed of 300,000 liters/sec on xenon. Grafoil® sputter suppression material lines the interior wall. Pressure measurements were made near the midpoint of the chamber's side wall using a screen-mesh-shielded ionization pressure gauge calibrated on air.

Tests at PEPL were performed in the 9-m long by 6-m diameter stainless-steel clad Large Vacuum Test Facility (LVTF). The LVTF uses four LN2-cooled CVI TM1200 reentrant cryopumps, giving a measured xenon pumping speed of 140,000 l/s. The chamber has a louvered 1.8-m by 1.8-m graphite beam dump in the center of the end cap, downstream of the thruster plume. Pressure measurements were made near the midpoint of the chamber's side wall using an ionization pressure gauge calibrated on air.

Plume Characterization

The plume test series described here was designed to be a U.S. risk reduction experiment. A more extensive study was performed at Fakel by Kozubsky, et al.[3]

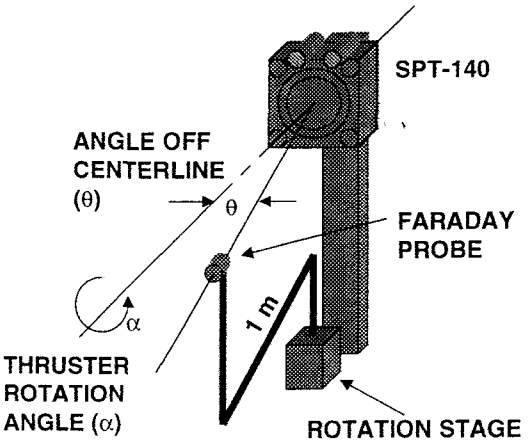

Fig. 2. Illustration of the orientations of the Faraday probe and thruster.

The measurements described here, performed at PEPL, consist primarily of ion current density. In addition, an attempt was made to measure far-field ion energy spectra. However, difficulty with spectrometer calibration precluded obtainment of accurate quantitative results.[4] Therefore, this paper will focus on the ion current density measurements.

Test Setup

Inside the LVTF at PEPL, the thruster was mounted on a stepper-motor-driven mechanism which could rotate the thruster about its centerline. The centerline of the thruster was in the horizontal plane, with the thruster exit toward the graphite beam dump on the back wall of the chamber.

The diagnostic setup was similar to those performed before at NASA GRC.[5,6]

The Faraday probe, provided by the Air Force Research Laboratory (AFRL), consisted of a molybdenum collector 0.75 inches in diameter surrounded by a molybdenum guard ring with an inner diameter of 0.85 inches and an outer diameter of 1.70 inches. A ring of Macor machinable ceramic electrically insulated the collector and guard ring. Fig. 1 is a photograph of the probe showing the center collector, guard ring, and outer Macor insulator. As Fig. 2 shows, the Faraday probe was oriented facing the center of the thruster exit plane, 1 m away. The probe was mounted on a vertical post, which was in turn mounted to a horizontal boom whose center of rotation was aligned with the exit plane of the thruster. This allowed the probe to be swept through a horizontal plane extending through the center of the thruster, at a constant radius, ±100 degrees off centerline. The uncertainty in the probe angle was ±2 degrees.

(c)2000 American Institute of Aeronautics & Astronautics or Published with Permission of Author(s) and/or Author(s)' Sponsoring Organization.

The Faraday probe collector and guard ring were each biased to -15 V using separate power supplies. A 40-Ω shunt was placed between the collector and its power supply. The voltage across the shunt was measured on an AM 501 operational amplifier attached to a Tektronix TDS 540 oscilloscope.

Test Procedure

The SPT-140 was operated at constant 300V discharge. By varying the propellant flow rate, three power settings were tested: 2, 3, and 4.5 kW. At each power setting, measurements were taken at 6 orientations of the thruster rotated about its centerline: α = -60, -30, 0, 30, 60, and 90 degrees. Rotation is positive counterclockwise looking at the thruster face, and, at zero degrees, the cathodes are on top of the thruster. At each power setting and thruster rotational orientation, Faraday probe sweeps were performed for $-100 < \theta < 100$ degrees off thruster centerline, at 1-degree increments.

Results and Discussion

The chamber pressures were 8.3×10^{-6}, 1.2×10^{-5} and 1.6×10^{-5} Torr (xenon) at 2, 3, and 4.5 kW powers, respectively.

Fig. 3 shows the ion current densities measured 1.0 m from the thruster exit. For off-axis angles less than approximately 30 degrees, decay of ion current density is exponential with θ. The instrumentation measurement uncertainty was estimated to be 3% for the majority of the ion current density values, dominated by calibration processes. However, in the tails of Fig. 3, for ion current densities less than about 0.2 mA/cm^2, discretization error begins to dominate, increasing the measurement uncertainty to approximately 7 μA/cm^2, or 6%, in those regions. It should be noted that these values strictly represent the uncertainty introduced by the measurement devices. As will be explained below, the uncertainty in the estimate of emitted ion beam current may be much higher due to ambient charge exchange plasma.

For all of the cases, very little (less than 1 degree) rotational asymmetry is seen. However, a common beam offset of approximately 2 degrees is apparent. This appears regardless of rotation, indicating that this offset is due to angular position error of the Faraday probe swing-arm, which was aligned to ±2 degrees.

An estimate of the total ion beam current can be obtained by integration of the curves in Fig. 3 as,

$$I_B = 2\pi r^2 \int_0^{\pi/2} j(\theta)\sin(\theta)d\theta\,, \qquad (1)$$

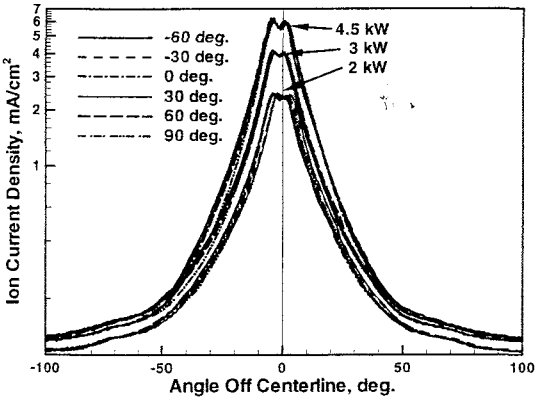

Fig. 3. Measured ion current density 1m from thruster exit at 2, 3, and 4.5kW discharge power.

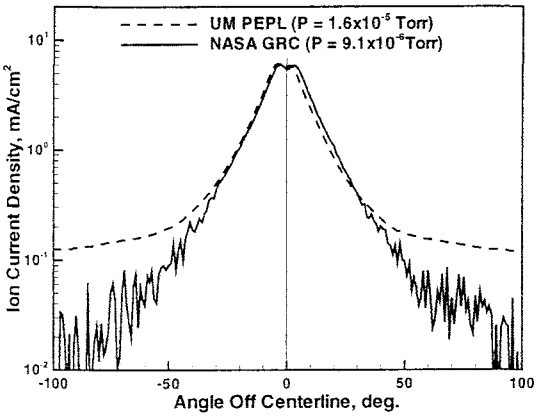

Fig. 4. Comparison of NASA GRC and UM PEPL ion current density measurements 1m from thruster exit at 4.5kW discharge power. α = 0 deg.

where r is the radial distance from the thruster exit to the Faraday probe, j is the measured ion current density, and θ is the angle off-centerline. For 2, 3, and 4.5 kW, I_B is found (using the trapezoidal rule) to be 13.2, 17.1, and 21.8 Amperes, respectively. These values are approximately twice the expected beam currents, which are 5.0, 7.8, and 11.4 Amperes, calculated by estimating a propellant utilization of 94%[7] a double-ion fraction of 0.04,[7] and a cathode flow fraction of 5%. This discrepancy has been studied before,[8] and is believed to be due to additional collection of ambient low-energy charge exchange ions that we will call j_a. To first order, assuming j_a is constant versus θ, j_a must be 0.131, 0.148, and 0.166 mA/cm^2 for 2, 3, and 4.5 kW, respectively. This is a significant fraction of the ion current density in the extremities of the beam for $|\theta| > 40°$, but is small compared to the measured values near centerline.

Current-density data at 4.5 kW and α = 0 degrees were also acquired as a part of the performance testing at GRC, where the chamber pressure at this power level

(c)2000 American Institute of Aeronautics & Astronautics or Published with Permission of Author(s) and/or Author(s)' Sponsoring Organization.

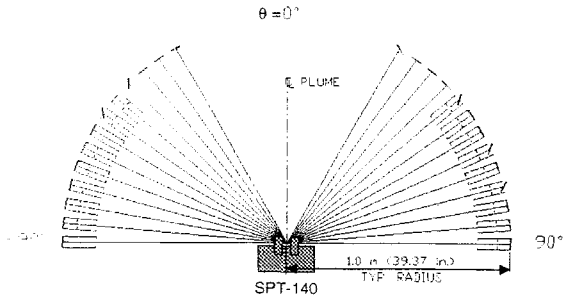

Fig. 5. Illustration of the placement of exposure samples with respect to the SPT-140.

was nearly a factor of two lower than at PEPL. The Faraday probe used in the GRC tests had the same collector dimensions, collector material, and electrical bias as the AFRL probe. Fig. 4 shows data from both facilities at the same thruster operating condition. Note that neither data set has been corrected for probe offset from the thruster centerline, thus they appear to be shifted from each other. In the plume core, the data are very similar. Farther from the thruster centerline, where charge-exchange plasma would be expected to dominate, the GRC data are much lower (though noisier) than the PEPL data. This comparison supports the hypothesis that the additional current collected was due to ambient charge-exchange ions, which would be expected to decrease with decreasing chamber background pressure. Integration of the GRC Faraday probe data yields I_B = 16.6 A, much smaller than the PEPL data, yet still larger than the expected beam current.

Sputtering and Contamination

The sputtering and contamination test was performed in VF6 at NASA GRC. The test involved placement of sputtering targets 1 m from the thruster exit at various off-axis angles and at various angles of incidence. Thruster firing duration was 100 hours at 3 kW.

Test Setup

The sputtering and contamination test setup was similar to one used previously by E. Pencil et al. at GRC.[9] It consisted of various 4-cm^2 samples, most of which were enclosed in collimators, affixed to a 1-m-radius semicircle as shown in Fig. 5. The semicircle placed the collimators in the horizontal plane bisecting the thruster plume. The actual samples, after mounting, were 1.0 m ±1 cm from the thruster exit. The stainless steel semicircle frame was covered with Grafoil® sputter suppression material.

The samples were secured to a metallic holder and masked by tantalum foil so that approximately 2 cm^2 of area was exposed. Most of the sample holders were placed in collimators that had two circular molybdenum apertures located 5.72 and 15.24 cm in front of the sample. The aperture diameters were 2.69 and 3.83 cm in diameter, respectively. The collimator axes were aligned radially toward the center of the thruster exit plane.

Four sample types were tested: solar cell cover glass, RTV silicone, Kapton®, and optical solar reflector (OSR). Table 1 shows where each sample was placed, its angle of incidence to the beam, and whether or not it was placed in a collimator.

Collimators were aligned on the semicircle and tested

Table 1. Sample type, off-axis angle (θ), angle of incidence (ϕ) to the ion beam, and mount type.

θ (deg)	ϕ (deg)	Sample Type	Collimator (Y/N)
-90	0	Cover Glass	Y
-85	0	Cover Glass	Y
-80	0	Cover Glass	Y
-75	0	Cover Glass	Y
-70	0	Cover Glass	Y
-65	0	Cover Glass	Y
-60	0	Cover Glass	Y
-55	45	OSR	Y
-50	0	Cover Glass	Y
-45	45	RTV	N
-40	0	Cover Glass	N
-35	0	Kapton®	N
-30	0	Cover Glass	N
30	30	Cover Glass	N
35	0	OSR	N
40	0	RTV	N
45	0	RTV	N
50	60	Cover Glass	Y
55	0	OSR	Y
60	0	Kapton®	Y
65	45	Cover Glass	Y
70	0	RTV	Y
75	45	Cover Glass	Y
80	0	OSR	Y
85	0	OSR	Y
90	0	OSR	Y

Table 2. Measurement matrix for exposure samples. B = Before , A = After exposure

Test	Cover Glass	RTV Silicone	Kapton®
Mass	B,A	B,A	B,A
Profilometry	A	A	A
Transmittance	B,A		

(c)2000 American Institute of Aeronautics & Astronautics or Published with Permission of Author(s) and/or Author(s)' Sponsoring Organization.

by ensuring that the beam of a pen-laser in a modified collimator fell within 2 mm of the semicircle center. The alignment of the finished assembly with the thruster was validated by using the collimator/laser to illuminate points on the thruster side and face. The accuracy of this alignment is estimated to be ± 1.3 deg.

In addition to the samples placed on the semicircle assembly, one of each type of sample was used as an in-chamber control and placed in a vented aluminum box 8 m behind the thruster. Also, one of each type of sample was used as a laboratory control outside the vacuum chamber.

Test Procedure

Pre- and post-exposure sample evaluation was conducted according to the matrix in Table 2. Additional measurements were made (not shown in Table 2), which are presented in a report by Jaworske.[10] OSR sample evaluations were performed outside GRC, and do not appear in Table 2.

Mass measurements of the cover glass samples were made using a Mettler M 3 scale, and were assumed accurate to ±0.000001 g, based on the instrument specifications. The masses of the RTV and Kapton® samples were out of range of the Mettler M 3, and were measured using a Sartorius R160P scale, accurate to ±0.00001 g. Before weighing, Kapton® samples were desiccated for 24 hours at 20 mTorr at ambient temperature. Cover glass and RTV were not desiccated.

Surface profilometry using a Dektek II was performed after plume exposure to identify contaminant thickness and/or erosion loss. Minimum detectable step height using this technique was 10 nm based on calibration of the instrument with standard steps. The height of the step was measured at the edge of the exposed region.

Solar transmittance with respect to the air mass zero solar spectrum was obtained to ±0.002 before and after plume exposure using a Perkin-Elmer Lambda-19 spectrophotometer equipped with a 15 cm diameter integrating sphere.

After the samples were pre-tested according to Table 2 and mounted in holders, the unmasked area (i.e. the area exposed to the thruster plume) was estimated by photographic comparison to a calibration image. The uncertainty introduced by this method was estimated to be 1%.

After photographic area estimation, exposure samples and in-chamber controls were installed in VF6. Thruster operation began after overnight pumping, and lasted for 100 hours. After cool-down and re-

Table 3. Mass loss, erosion depth, and change in total transmittance (ΔTT) for normal-incidence cover glass exposure samples after 100 hours.

θ (deg)	Mass Loss (g/cm^2)	Erosion (nm)	ΔTT
-90	-2.82×10^{-7} $\pm1.4\times10^{-5}$	30 ±13	0.006 ±0.002
-85	3.30×10^{-5} $\pm1.4\times10^{-4}$	43 ±16	0.002 ±0.002
-80	-5.43×10^{-6} $\pm1.4\times10^{-5}$	36 ±15	-0.003 ±0.002
-75	3.44×10^{-5} $\pm1.4\times10^{-5}$	190 ±58	-0.036 ±0.002
-70	4.83×10^{-5} $\pm1.4\times10^{-5}$	140 ±43	-0.045 ±0.002
-65	3.74×10^{-5} $\pm2.7\times10^{-5}$	210 ±64	-0.057 ±0.002
-60	1.48×10^{-4} $\pm1.7\times10^{-5}$	380 ±110	-0.0041 ±0.002
-50	9.46×10^{-4} $\pm1.9\times10^{-5}$	3850 ±1200	-0.012 ±0.002
-40	2.93×10^{-3} $\pm3.2\times10^{-5}$	12000 ±3600	-0.012 ±0.002
-30	6.81×10^{-3} $\pm7.8\times10^{-5}$	24200 ±7300	-0.006 ±0.002

Table 4. Mass loss and erosion depth for additional samples after 100 hours.

θ (deg)	ϕ (deg)	Mass Loss (g/cm^2)	Erosion (nm)
Cover Glass			
30	30	9.14×10^{-3} $\pm9.2\times10^{-5}$	37900 ±11000
50	60	1.14×10^{-3} $\pm1.8\times10^{-5}$	4960 ±1500
65	45	3.42×10^{-4} $\pm5.3\times10^{-5}$	1060 ±320
75	45	1.13×10^{-3} $\pm1.4\times10^{-5}$	350 ±100
RTV Silicone			
-45	45	2.50×10^{-3} $\pm9.1\times10^{-5}$	21500 ±6500
40	0	6.22×10^{-3} $\pm1.1\times10^{-4}$	18900 ±5700
45	0	2.45×10^{-3} $\pm9.0\times10^{-5}$	14100 ±4200
70	0	2.48×10^{-4} $\pm8.7\times10^{-5}$	- -
Kapton®			
-35	0	1.90×10^{-3} $\pm1.4\times10^{-4}$	18600 ±5600
60	0	2.77×10^{-4} $\pm1.4\times10^{-4}$	14000 ±4200

(c)2000 American Institute of Aeronautics & Astronautics or Published with Permission of Author(s) and/or Author(s)' Sponsoring Organization.

pressurization, post-testing was performed according to Table 2.

Results and Discussion

What follows is a short sampling of some of the results from the sputtering and contamination experiment. Additional information may be found in a report by Jaworske.[10]

During thruster operation, chamber background pressure was 6×10^{-6} Torr (xenon).

Table 3 shows the mass loss, erosion depth, and change in total transmittance for the normal-incidence solar cell cover glass exposure samples only. (Note that two of these samples, at -40 and -30 deg., were not in collimators.) Fig. 6 shows mass loss and erosion depth plotted versus off-axis angle.

Uncertainty in mass loss is dominated by three sources: outgassing, area estimation (1%), and breakage correction. The uncertainty values in Table 3 are the RMS-combined uncertainties of these three components, which are described below.

During post-test extraction of the samples from their holders, it was noticed that 8 of the samples (all cover glass) were adhered to their holder by epoxy which had been used to affix the molybdenum masks. Extraction from the holder required breakage of some of the corners of these samples (all in areas covered by the molybdenum mask). The missing mass was estimated using a photographic technique and added to the final mass. Uncertainty in this correction method was estimated using the statistics of multiple trials to be ~3%.

The in-chamber cover glass control sample lost 0.022 mg during the 100-hour test, presumably to outgassing. Assuming this loss to be 50% probable in a normal distribution, uncertainty (standard deviation) is found to be 1.4×10^{-5} g/cm^2 for all samples.

Outgassing and breakage correction dominate the uncertainty calculation for most of the samples, except for $|\theta| < 50$ degrees, where the 1% area measurement uncertainty is most significant. For $|\theta| > 60$ degrees, the uncertainty is of the same order as the measurement. Precision of similar mass loss experiments in the future may be improved by increasing the firing duration and attempting to account for outgassing as systematic error.

Erosion depth, given in Table 3 and Fig. 6, is seen to follow the same trend as mass loss. Calibration of the profilometer was based on measurement of two standard steps. For well-defined steps such as the calibration standards, the profilometer yields accurate

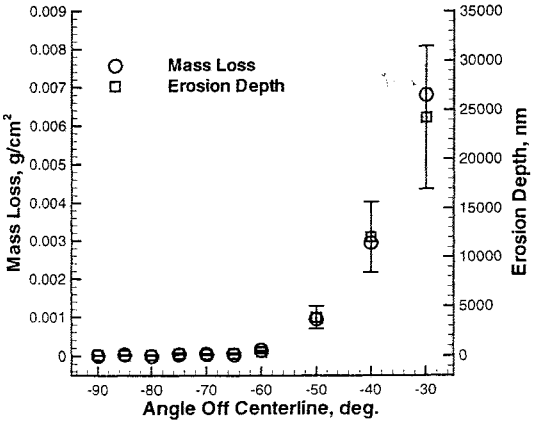

Fig. 6. Erosion depth and mass loss for 100-hour cover glass exposure samples.

step height value ±10 nm. For less well-defined steps, it was necessary to measure the topography in the vicinity of the step, and estimate an idealized step height. In these cases, the step height was estimated using an extrapolation technique which had an accuracy of ±30%.

As a check on mass loss and step height measurements, the sample density was estimated by dividing the mass loss per unit area by the step height. The mean result for the seven innermost samples (i.e. those where there was net erosion) was 2.66 g/cm^3, which is very close to the known cover glass density of 2.61 g/cm^3.

Table 3 also shows the change in total transmittance of the samples during the exposure test. Positive ΔTT values represent an increase in total transmittance. The mean and standard deviation in total transmittance before exposure were 0.7873 and 0.0015, respectively. Uncertainty is taken to be the rated instrument accuracy of ±0.002.

Results from the RTV, Kapton®, and canted cover glass samples are listed in Table 4. Erosion depth is not given for the RTV sample at 70 deg. because the step height was found to be on the order of the surface roughness. No results appear for the OSR samples because they are being analyzed outside GRC, and data were not available in time for inclusion in this paper.

Electromagnetic Interference

The EMI test was performed at VF6 at NASA GRC and involved measurement of radiated EMI emissions based upon MIL-STD-462 with modifications specific to the SPT-140. Data are presented in comparison to MIL-STD-461 specifications.

(c)2000 American Institute of Aeronautics & Astronautics or Published with Permission of Author(s) and/or Author(s)' Sponsoring Organization.

Test Setup

The EMI test setup was similar to ones used previously at GRC.[11,12]

A portable EMI test pallet was positioned near the middle of the VF6 chamber. It served as a base upon which supports for the thruster and measurement antennas were fixed, as shown in Fig. 6. Atop a 1.4 m aluminum post attached to the front edge of the EMI pallet, the thruster was mounted with its centerline 0.9 m below the chamber midpoint, and its beam directed axially toward the pumping end of the chamber. E-field sensing antennas were arrayed in a 1-m radius semicircle behind the thruster exit plane. Each antenna was mounted using fiberglass supports to minimize scattering. A Kapton® tent was erected to enclose the array but exclude the thruster, so that plasma environment effects on the antenna properties were mitigated. A 14-cm diameter loop antenna for the H-field emission measurement was fixed coaxial to the thruster centerline 7 cm behind the back face of the thruster. Residing outside the main Kapton® tent, the H-field loop was enclosed by a separate Kapton® envelope to likewise prevent plasma impingement.

All thruster power supplies were located outside the vacuum chamber and fed through via twisted pair, shielded cables. Antennas were connected via low-loss coaxial cable to EMI receiving equipment located immediately outside the tank feedthrough closest to the antenna array. This included an H.P. 8566B (superheterodyne-type, harmonically mixed) spectrum analyzer with 85685A preselector and a switch bank of low noise amplifiers (LNAs) used to boost sensitivity at frequencies above 1 GHz. Each cable/filter/LNA/switch path had been calibrated for net gain/loss vs. frequency prior to testing.

Test Procedure

Software was used to automatically set analyzer parameters and perform frequency sweeps. The spectrum analyzer was operated in peak detection mode for all measurements. This captured an envelope of the peaks, or noise fluctuation maxima, present during a given sweep (in time or frequency domain). Wide frequency ranges were assembled from a composite of many individual sweeps covering smaller frequency spans (Table 5).

To give a background emission reference, full E-field (MIL-STD-461C, RE02) and H-field (MIL-STD-461D, RE101) sweeps were performed at vacuum with the SPT-140 in an OFF state and unpowered. The sweeps were repeated for two steady state thruster operating points, designated by the discharge powers of 3 and 4.5 kW.

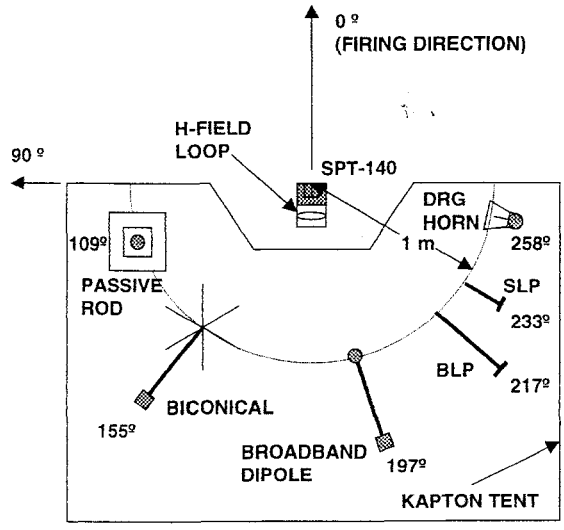

Fig. 7. Top view of EMI pallet.

Table 5. Antennas and broadband measurement bandwidths.

Freq. (Hz)	Antenna	Sweep Resolution Bandwidth (Hz)
E-Field		
10k-250k	Passive Rod Band 1	3k
250k-500k	Passive Rod Band 2	3k
500k-1M	Passive Rod Band 3	10k
1M-2M	Passive Rod Band 4	10k
2M-4M	Passive Rod Band 5	10k
4M-8M	Passive Rod Band 6	30k
8M-16M	Passive Rod Band 7	30k
16M-32M	Passive Rod Band 8	30k
32M-200M	Biconical	100k
200M-350M	Broadband Dipole	300k
350M-1G	BLP	300k
1G-2G	DRG Horn	3M
2G-4G		3M
4G-8G		3M
8G-18G		3M
B-Field		
30-1k	Loop (14 cm dia.)	10
1k-10k		100
10k-100k		1k

Results and Discussion

During thruster operation, the background pressures were 7.2×10^{-6} and 9.3×10^{-6} Torr (xenon) at 3 and 4.5 kW, respectively.

Fig. 8 and Fig. 9 show the measured E-field emission with the thruster OFF (background) and ON,

(c)2000 American Institute of Aeronautics & Astronautics or Published with Permission of Author(s) and/or Author(s)' Sponsoring Organization.

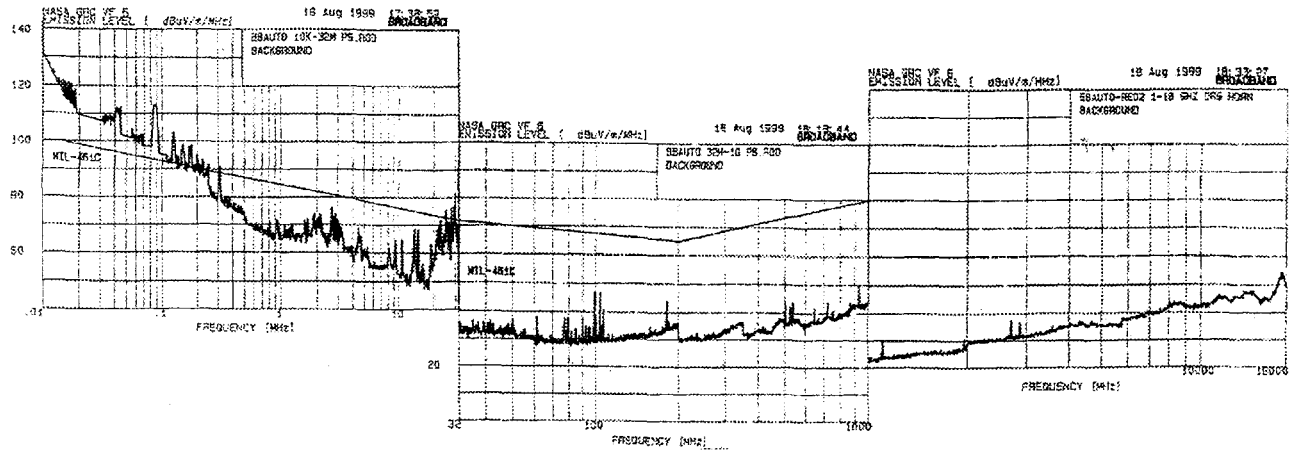

Fig. 8. E-field background/sensitivity threshold. (Note horizontal scale changes at breakpoints.)

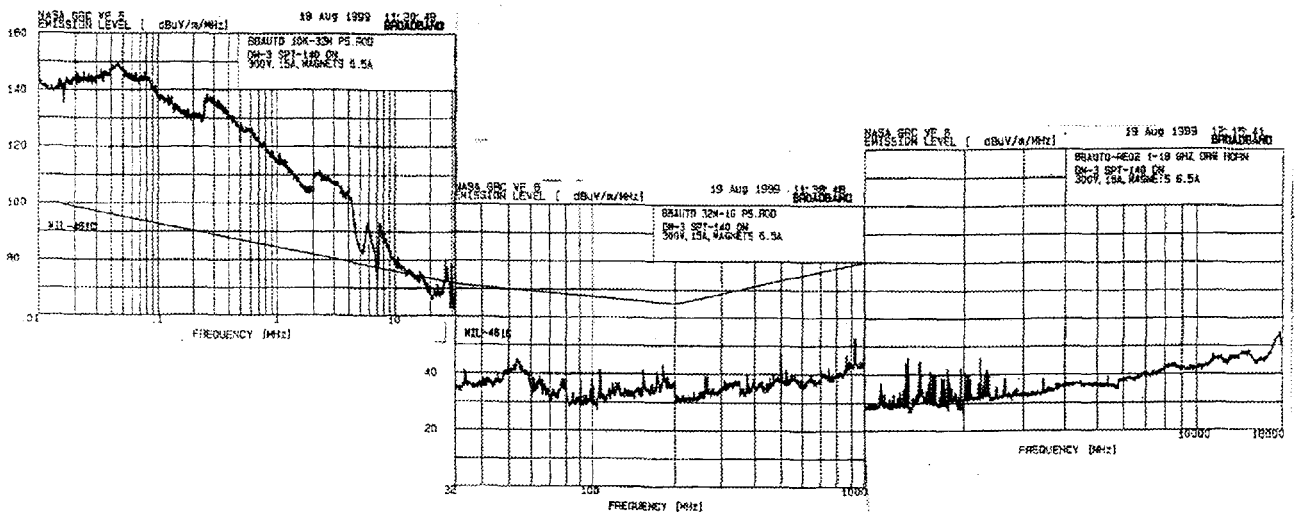

Fig. 9. E-field emissions for thruster firing at 4.5 kW. (Note horizontal scale change at breakpoints.)

respectively. Although the 3 kW and 4.5 kW data were similar, the 4.5 kW emissions were, in general, slightly greater than the 3 kW emissions. Therefore, only the 4.5 kW data will be shown in this report.

Thruster E-field emissions exceeded background levels or the sensitivity threshold in the following frequency ranges:

- 10 kHz to 20 MHz
- 32 MHz to 80 MHz
- 1 GHz to 3 GHz

In the 32 to 80 MHz range, several distinct bands of radiated emission are apparent, with a maximum level of 44 dBμV/m/MHz at 55 MHz. However, all detected emissions in this range fall beneath the MIL-STD-461C specification. In the range 10 kHz to 20 MHz, however, broadband incoherent-type emissions exceed MIL-STD-461C specifications by up to 53 dB at 45 kHz for the applied worst-case or coherent-type *20log* bandwidth normalization. (The actual emission level corresponding to an incoherent or *10log* bandwidth normalization would exceed the limit by just 29 dB.)

The SPT-140 was found to emit aperiodic broadband emissions at levels above detection threshold from 1 to 3 GHz. As no MIL-461C broadband limit exists above 1 GHz, comparison against this general standard is not apparent.

Fig. 10 shows the measured H-field emission detected by the 14-cm loop antenna. Like the E-field emission, the 4.5 kW emissions are the highest, and are presented as the worst case.

Thruster H-field emissions were broadband in nature for the MIL-461D specified measurement bandwidths, and exceeded the background for frequencies greater than 300 Hz. The highest emission levels were reached at ~20 kHz, which corresponded to the

(c)2000 American Institute of Aeronautics & Astronautics or Published with Permission of Author(s) and/or Author(s)' Sponsoring Organization.

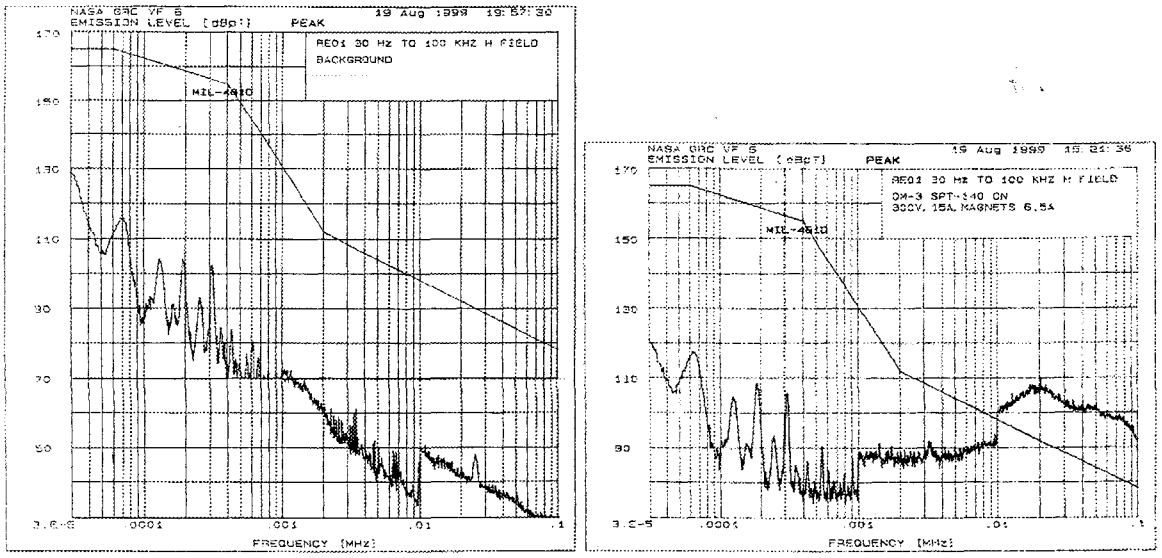

(a) (b)

Fig. 10. H-field emissions from 30 Hz to 100 kHz. a) background b) during thruster firing at 4.5 kW.

frequency of observed discharge current oscillations. Emissions exceeded the MIL-461D RE101 limit by up to 18 dBpT at frequencies from 10 to 100 kHz.

Summary

Ion current density measurements showed near-exponential decay with off-axis angle up to approximately 30 degrees. At off-axis angles greater than 30 degrees, results varied with chamber background pressure, presumably due to ambient charge exchange plasma. No significant change in the current density was observed for varying rotation angles about the thruster centerline.

Sputtering and contamination tests quantified the erosion depth, mass loss, and solar transmittance of several materials accurately for off-axis angles less than approximately 60 degrees. At off-axis angles greater than 60 degrees, the sputter rate was on the order of the measurement uncertainty. Although uncertainty is high for large off-axis angles, erosion depth and mass loss measurements follow expected trends, and are in agreement with each other.

EMI tests found one band of low-frequency emission (10 kHz to 20 MHz) which exceeded the MIL-STD-461C specification by up to 53 dB. However, this is outside the traditionally important RF communications bands.

References

[1]Oleson, S. R. and R M. Myers, "Launch Vehicle and Power Level Impacts on Electric GEO Insertion," AIAA-96-2978, 32nd AIAA/ASME/SAE/ASEE Joint Propulsion Conference, Lake Buena Vista, FL, July 1996.

[2]Hargus, W. A. et al., "Preliminary Performance Results of the High Performance Hall System SPT-140," AIAA-2000-3250, 36th AIAA/ASME/SAE/-ASEE Joint Propulsion Conference, Huntsville, AL, July 2000.

[3]Kozubsky, K., Kudriavtzev, S., and S. Pridannikov, "Plume Study of Multimode Thruster SPT-140," IEPC-99-073, 26th International Electric Propulsion Conference, Kitakyushu, Japan, October, 1999.

[4]Hofer, R., Haas, J., and A. Gallimore, "Development of a 45-degree Parallel-plate Electrostatic Energy Analyzer for Hall Thruster Plume Studies: Preliminary Data," IEPC-99-113, 26th International Electric Propulsion Conference, Kitakyushu, Japan, October, 1999.

[5]Myers, R. M. and D. H. Manzella, "Stationary Plasma Thruster Plume Characteristics," IEPC-93-096, 23rd International Electric Propulsion Conference, Seattle, WA, September, 1993.

[6]Manzella, D. H. and J. M. Sankovic, "Hall Thruster Ion Beam Characterization," AIAA-95-2927, 31st AIAA/ASME/SAE/ASEE Joint Propulsion Conference, July, 1995.

[7]Fife, J. M., "Hybrid-PIC Modeling and Electrostatic Probe Survey of Hall Thrusters," PhD Thesis,

(c)2000 American Institute of Aeronautics & Astronautics or Published with Permission of Author(s) and/or Author(s)' Sponsoring Organization.

Massachusetts Institute of Technology, September 1998.

[8]de Grys, K. H., Tilley, D. L., and R. S. Aadland, "BPT Hall Thruster Plume Characteristics," AIAA-99-2283, 35th AIAA/ASME/SAE/ASEE Joint Propulsion Conference and Exhibit, Los Angeles, California, June 1999.

[9]Pencil, E., Randolph, T, and D. Manzella., "End-of-life Stationary Plasma Thruster Plume Characterization," AIAA-96-2709, 32nd AIAA/ASME/SAE/ASEE Joint Propulsion Conference, July 1996.

[10]Jaworske, D. A., "Hall Effect Thruster Plume Contamination and Erosion Study," NASA Technical Memorandum, NASA/TM-2000-210204.

[11]Sarmiento, C. et al., "RHETT2/EPDM Hall Thruster Propulsion System Electromagnetic Compatability Evaluation," IEPC-97-108, Proceedings of the 25th International Electric Propulsion Conference, August, 1997.

[12]Manzella, D. et al., "Performance Evaluation of the SPT-140," IEPC-97-059, 25th International Electric Propulsion Conference, Cleveland, Ohio, August, 1997.